

One-step Hydrothermal Synthesis of Sn-doped OMS-2 and Their Electrochemical Performance

Ming Sun, Fei Ye, Bang Lan, Lin Yu*, Xiaoling Cheng, Shengnan Liu, Xiaoqing Zhang

School of Chemical Engineering and Light Industry, Guangdong University of Technology, Guangzhou 510006, P. R.China

*E-mail: gych@gdut.edu.cn; sunmgz@gmail.com

Received: 5 August 2012 / Accepted: 12 September 2012 / Published: 1 October 2012

Different amount of Sn doped manganese oxide octahedral molecular sieve (OMS-2) were synthesized by one-step hydrothermal method using SnCl_4 , MnSO_4 and KMnO_4 as raw materials. The Sn-OMS-2 materials were characterized by X-ray diffraction (XRD), Raman spectra, Uv-vis spectra, scanning electron microscopy (SEM), energy dispersive X-ray analysis (EDX), transmission electron microscopy (TEM) and surface area analysis. The XRD, Raman and UV-Vis analysis confirm the cryptomelane-Q type of MnO_2 crystal structure and no extra peaks related to tin metal or impurities were observed. SEM and TEM images show the nanorod morphology of the materials. EDX result proves that Sn has been successfully doped into the OMS-2 structure. The supercapacitive performances of Sn-OMS-2 materials were tested using cyclic voltammetry (CV) and galvanostatic charge-discharge techniques in 1M Na_2SO_4 electrolyte under different scan rate. Improvement in capacitance of the OMS-2 materials is observed after doping with Sn, and increased with the Sn dopant rise, of which 15%Sn-OMS-2 sample exhibited the best supercapacitive property (187 F/g).

Keywords: Manganese oxide octahedral molecular sieve, doping tin, hydrothermal synthesis, capacitance property

1. INTRODUCTION

The electrochemical capacitors (ECs) or super capacitors have received significant interests for their high capacity, high power density, and long cycle life as one kind of energy storage devices[1]. Generally, the electrode materials for ECs include carbon-base materials (e.g. carbon blacks, carbon nanotube, activated carbon, etc.), conductive polymers (e.g. polyaniline, polypyrrole, polythiophene, etc.) and transition metal oxides [1], of which the transition metal oxides are considered as the less expensive and promising candidates for ECs electrode materials. The transition metal oxides studied up to now include NiO , SnO_2 , Co_3O_4 , V_2O_5 and manganese oxide (MnO_x) [2, 3].

Due to their low cost and high specific capacitance in aqueous electrolyte, environmentally friendly manganese oxides have attracted wide attentions as active electrode materials for ECs [4]. Manganese oxides exist in polymorphic structure such as α -, β -, γ -, δ -type based on the different configuration of the basic $[\text{MnO}_6]$ octahedral unit [5]. Cryptomelane-type manganese oxide, also called as manganese oxide octahedral molecular sieve (OMS-2), has a formula of $\text{KMn}_8\text{O}_{16}$. OMS-2 is one type of manganese oxides which has a 2×2 tunnel structure with a pore size of 0.46 nm and find wide applications in many fields. The crystalline structure, the size and morphology of manganese oxides have great influence on their electrochemical performance [6, 7]. Therefore, great efforts have been devoted on the preparation of various types of manganese oxides with different morphology and surface area.

Although manganese oxides have shown excellent pseudocapacitive performance, nevertheless, large electron transfer resistance in the redox process hinders their potential applications [2]. To solve the problem and improve the performance, the addition of other metal or metal oxides have been tried [4]. The incorporation of Fe [8], Ni [9], Co [10], Cr [11], V [12], Mo [13], Ag [14], Ru [15] oxides and Al [16], Sn [17], Pb [18] metal could effectively enhance the specific capacitances of Mn-based oxides.

SnO_2 is a semiconductor material which exhibits unique properties in lithium ion battery and supercapacitor [19, 20]. Tin oxide can also be used as a promoter for MoO_x and RuO_2 based electrochemical supercapacitors [21, 22]. However, few research papers have been published on the SnO_2 modified OMS-2 supercapacitor [23]. In view of the excellent conductivity of SnO_2 , herein, Sn-doped OMS-2 nanorod materials were prepared via one-step hydrothermal route using SnCl_4 , MnSO_4 and KMnO_4 as raw materials. The effects of Sn doping on the structure, morphology and electrochemical properties have been investigated thoroughly by comprehensive characterizations.

2. EXPERIMENTAL

2.1 Preparation process

All the chemical reagents were analytical grade and used as received. To synthesize Sn doped OMS-2, SnCl_4 , MnSO_4 (7.4 mmol) and KMnO_4 (5.6 mmol) were put into 18 ml distilled water adjusted by concentrated nitric acid, then transferred into a Teflon-lined stainless steel autoclave, sealed and maintain at 160 °C for 24 h. After the reaction was complete, the solid precipitate was washed with distilled water until pH=7, and then dried at 60 °C for 12 h to get the final product. The samples were denoted as x%Sn-OMS-2, of which x stands for the mole ratio of Sn to Mn in the raw materials.

2.2 Characterization

X-ray powder diffraction (XRD) was obtained on a MSAL-XD2 X-ray diffractometer operating at a voltage of 40 kV and a current of 25 mA with Cu $K\alpha$ radiation. The data were collected

at room temperature with a 0.01° step size in 2θ , from $2\theta = 10$ to 80° . The Raman spectra were recorded in a dispersive Horiva Jobin Yvon LabRam HR800 Microscope, with a 24 mW He-Ne green laser (633 nm) working at 0.24 mW power. The Raman spectrometer is calibrated using a silicon wafer. UV-Vis diffuse reflectance spectra were recorded with a Shimadzu UV-2450 spectrometer with an integrating sphere allowing scanning from 190 to 850 nm. BaSO_4 was used as a reference. Scanning electron microscopy (SEM) and was performed in a Digital Scanning Microscope S-3400N with an energy dispersive X-ray (EDX) analyzer operated at 15 kV. High resolution transmission electron microscopy (HRTEM) was performed on a Philips CM200-FEG electron microscope operated at an accelerating voltage of 200 kV. The Brunauer-Emmett-Teller (BET) surface area and micro-pore size distribution of the materials were measured by a multipoint N_2 adsorption-desorption method at liquid- N_2 temperature (-196°C) using an ASAP2020 surface area analyzer (Micromeritics, USA).

2.3 Electrochemical test

Electrochemical performance of the Sn-OMS-2 materials was evaluated in 1 M Na_2SO_4 electrolyte at room temperature, using a Solartron SI 1287 electrochemical interface and SI 1260 impedance/gain-phase analyzer. The test was performed in a three-electrode cell, in which Sn-OMS-2 electrode was assembled as the working electrode, a platinum mesh and a saturated calomel electrode (SCE) were used as the counter and the reference electrode, respectively. The working electrode was fabricated by compressing a mixture of the Sn-OMS-2, conductive agent acetylene black (AC), and binder polytetrafluoroethylene (PTFE) in a weight ratio of OMS-2: AC: PTFE 85:15:5 onto a foamed nickel with a dimension of $1\text{cm}\times 1\text{cm}$ at 0.2 MPa.

3. RESULTS AND DISCUSSION

3.1 Structure and Morphology Characterization

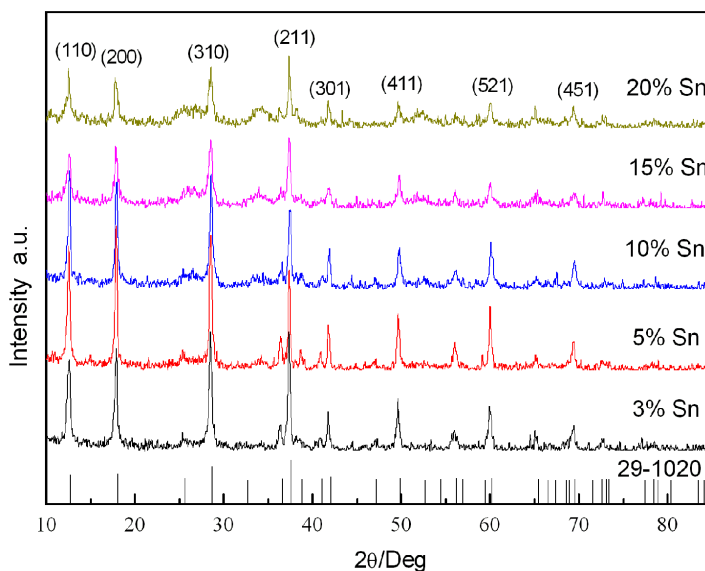


Figure 1. XRD patterns of the Sn-OMS-2 samples

The XRD patterns of the Sn-doped OMS-2 as shown in Fig.1 agree well with a cryptomelane structure characteristic for the octahedral molecular sieve material OMS-2. The peaks at $2\theta = 12.7, 18.0, 28.7, 37.6, 42.0, 49.8$ and 60.2 matched well with the patterns of synthetic cryptomelane-Q ($\text{KMn}_8\text{O}_{16}$, JCPDS 29-1020). For all the samples, no free SnO_2 or SnO or Sn metal phase were detected, indicating that tin cation are well-dispersed in the structure of the OMS-2 [24]. With increasing Sn dopant content, the XRD peaks become broad, and the peak intensity decrease, meaning that the particle size gets smaller.

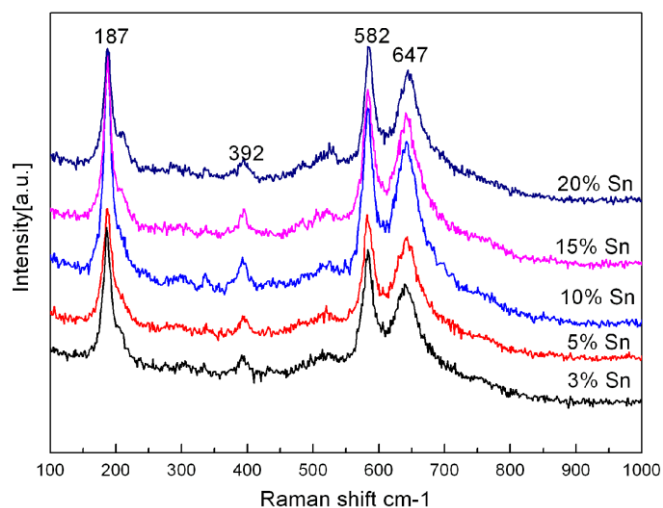


Figure 2. Raman spectra of the Sn-OMS-2 samples

To further confirm the structure of the prepared Sn-OMS-2 materials, Raman spectra were recorded in Fig.2. The Raman spectra were almost identical for all the samples, indicating that there were no structural changes with Sn dopant increasing. The Raman spectra of the Sn-OMS-2 samples feature four main bands at 187, 392, 582 and 647 cm^{-1} . The two sharp Raman bands at 582 and 647 cm^{-1} which are assigned to F_{2g} and A_{1g} species, respectively, are indicative of the vibration modes of $[\text{MnO}_6]$ octahedron [25]. No other peaks at around 476, 634, and 778 cm^{-1} corresponding to segregated SnO_2 were detected [26].

Figure 3 displays a continuous absorption in the UV and visible regions. The absorption can be seen as the overlap of three kinds of Mn peaks, as Mn in the OMS-2 crystallization has a mixed valence such as +2, +3 and +4. The band centered at about 250 nm is attributed to the charge transfer between oxygen anion and manganese cation (+2). The absorption at approximately 300 nm is associated with Mn^{4+} , and the continuous absorption is related to $\text{O}^{2-} \rightarrow \text{Mn}^{3+}$ charge transfer and d-d transition for a d^4 electronic configuration in an octahedral field [27]. For all the samples, no obvious changes can be found from the UV-Vis spectra.

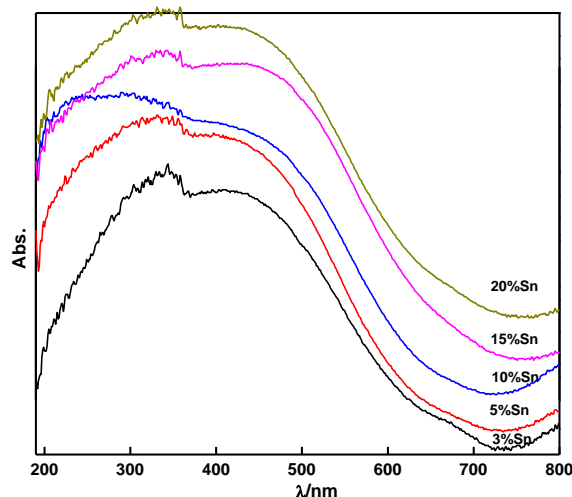


Figure 3. UV-vis spectra of the Sn-OMS-2 samples

The SEM micrographs (Fig.4) demonstrate that the Sn-OMS-2 samples consisted of similar stacked nanorod shape with the length in the range from dozens of nanometer to hundreds of nanometer. From the SEM image, we can also found that with Sn dopant rise, the length of the nanorods increase accordingly. To prove Sn was actually doped on the OMS-2 structure, the EDX characterization of 15%Sn-OMS-2 sample was taken as in Fig.4. The EDX spectrum shows peaks of O, K, Mn and Sn, of which the atom ratio of Sn to Mn is 0.152 close to the feeding material mole ratio (0.15).

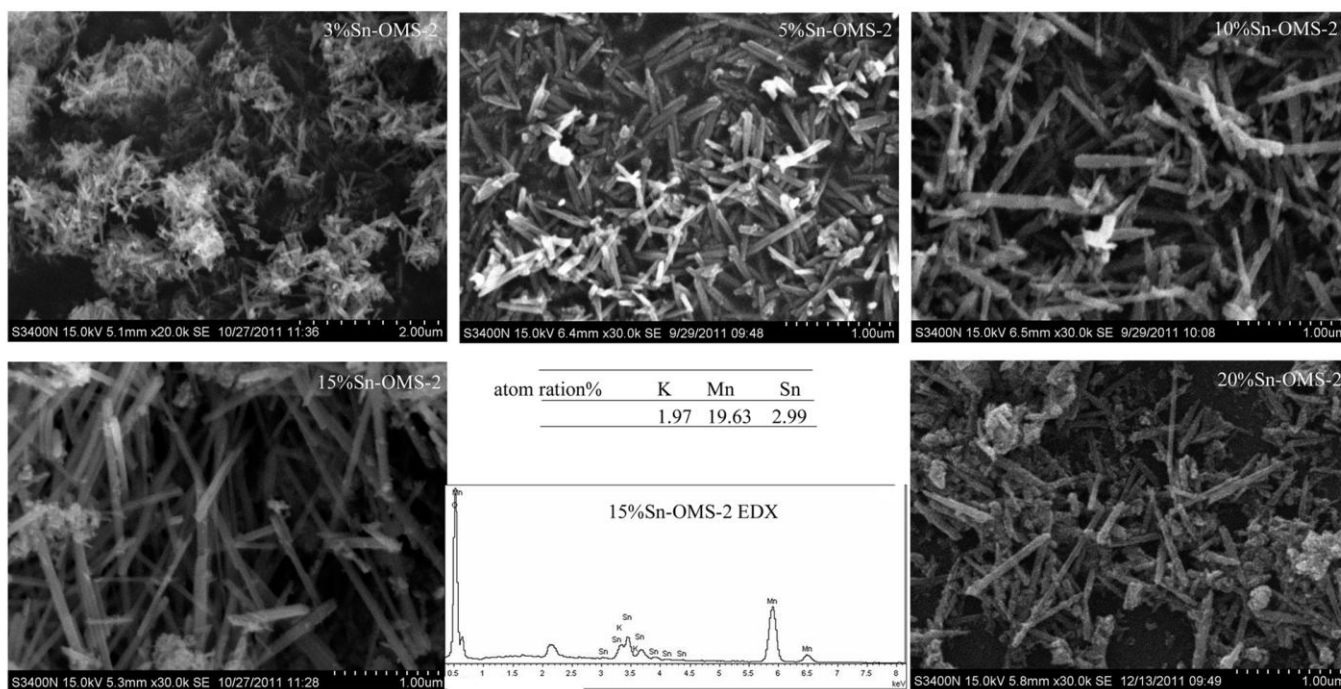


Figure 4. SEM images of the Sn-OMS-2 samples

The representative HRTEM of 15%Sn-OMS-2 sample were shown in Fig.5. From the inset Figure, we can see that the surface of the nanorod is not as smooth as pure OMS-2 reported elsewhere[28], but with defects and dislocations, and this may have potential influence on its activity. Tang et al.[29] also reported doped vanadium can induce surface defects of the OMS-2 materials. The separated spacing of 0.27 nm and 0.31 nm corresponds to (101) and (310) planes in the cryptomelane crystal structures.

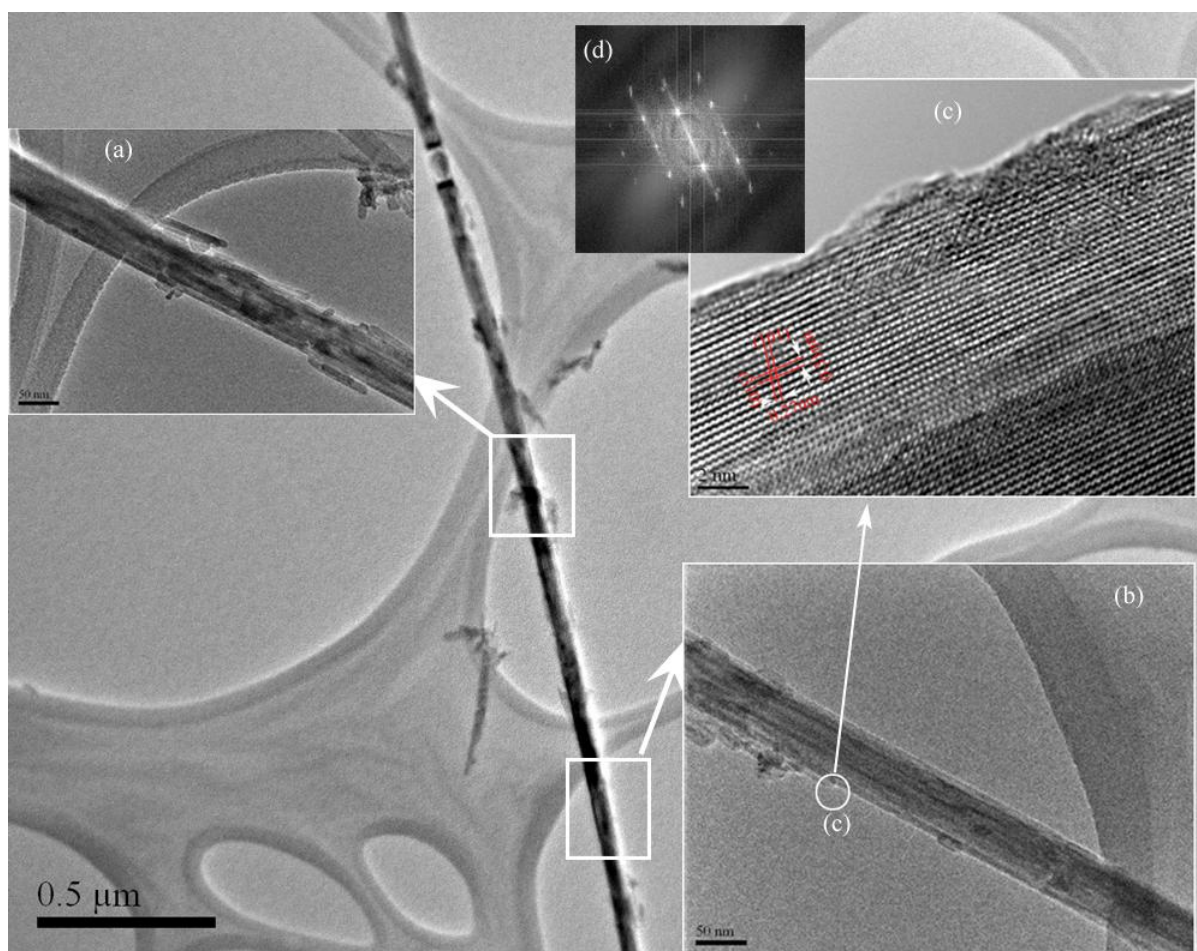


Figure5. HRTEM image of the 15%Sn-OMS-2 sample

The nitrogen adsorption-desorption isotherms of the materials were displayed in Fig.6. The isotherm is a characteristic of type II, with a hysteresis loop type H3 in the IUPAC classification, which is usually associated with the adsorption on aggregates of particles with a layered morphology, forming slit-like pores [30]. This type of isotherm is similar to that reported for OMS-2 material [31]. The Brunauer-Emmett-Teller (BET) surface area of the Sn-OMS-2 materials ranged from 48 to 108 m²/g and increased with Sn dopant rise. Fig.7 showed the micro-pore size distribution by Horvath-Kawazoe (H-K) method. All the materials exhibits microporous structure and Sn doping can decrease the micro pore size.

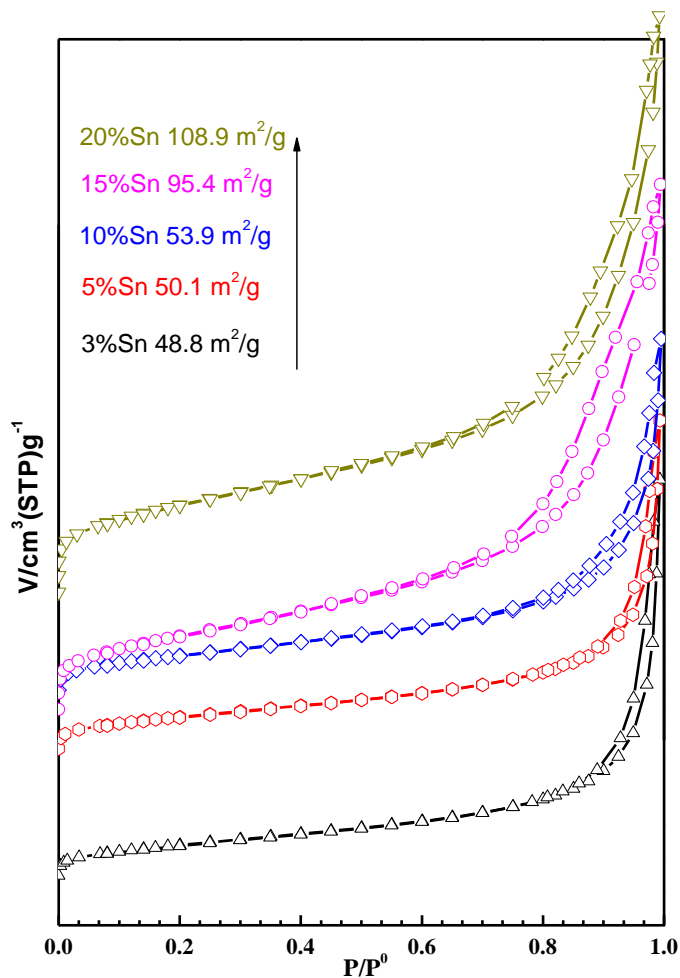


Figure 6. Nitrogen adsorption/desorption isotherms of the Sn-OMS-2 samples

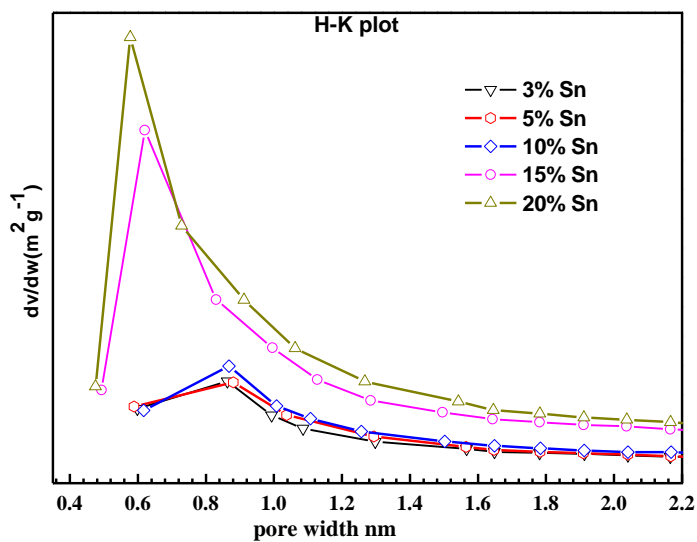


Figure 7. Micro pore-size distribution curves by H-K methods

3.2 Electrochemical Performance

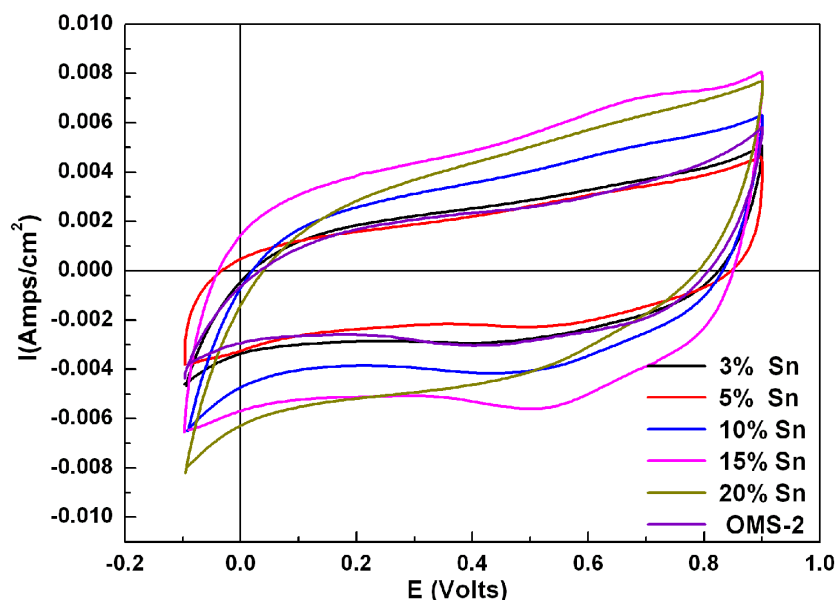


Figure 8. Cyclic voltammograms of Sn-OMS-2 materials in 1 M Na_2SO_4 at a scan rate of 10 mVs^{-1} (second cycle)

The cyclic voltammograms (CV) of different amount of Sn doped OMS-2 materials in Fig.8 show typical CV curves in potential range between -0.1 and +0.9 V. All the materials present almost rectangular shapes with the characteristic of electrochemical capacitive behavior, and no obvious redox peaks observed in the potential window range. From the symmetrically and steadily road current profiles, the CV curves exhibit typical pseudocapacitance characteristics. The area under the CV curves is in proportional to the specific capacitance. The capacitance calculated from the area of the CV curves was 85, 90, 89, 124, 187 and 146 F/g with Sn dopant rise from 0 to 20%. When the doping amount of Sn is below 5%, the capacitance of the Sn-OMS-2 is almost the same compared with that of the pure OMS-2 material. However, when the Sn dopant rise above 10%, the capacitance of Sn-OMS-2 materials improve a lot, of which the 15%Sn-OMS-2 sample show the best performance (187 F/g).

Two mechanisms have been advanced for the charge storage in manganese oxide electrodes [4, 32]. One is relied on the intercalation of electrolyte cations (such as Na^+ or K^+) in the bulk of manganese oxide. Another is the surface adsorption of electrolyte cations (such as Na^+ or K^+) on the manganese oxide. Based on the mechanisms, the specific capacitance relies on parameters such as crystallinity, surface area, and pore structure [2, 4, 33]. As seen from the Fig. 9, the OMS-2 material is constructed by double chains of $[\text{MnO}_6]$ forming 2×2 tunnels with K^+ in the tunnel to keep the tunnel structure stability [5]. As the radius of K^+ is larger than that of Na^+ or H^+ , during the reduction and deintercalation upon oxidation, the K^+ in the matrix tunnel can be easily substituted by the electrolyte cations of Na^+ or H^+ . Hence, the crystal tunnel structure favors for the capacitive property of Sn-OMS-2 materials. Thierry et al.[34] also reported that higher concentration of K^+ in the Binessite- MnO_2 can provide an additional capacitance. Because the conductivity of Sn is better than that of Mn, the Sn

dopant can improve the conductivity of OMS-2 electrode, leading to a rise in capacitance of the Sn-OMS-2 materials.

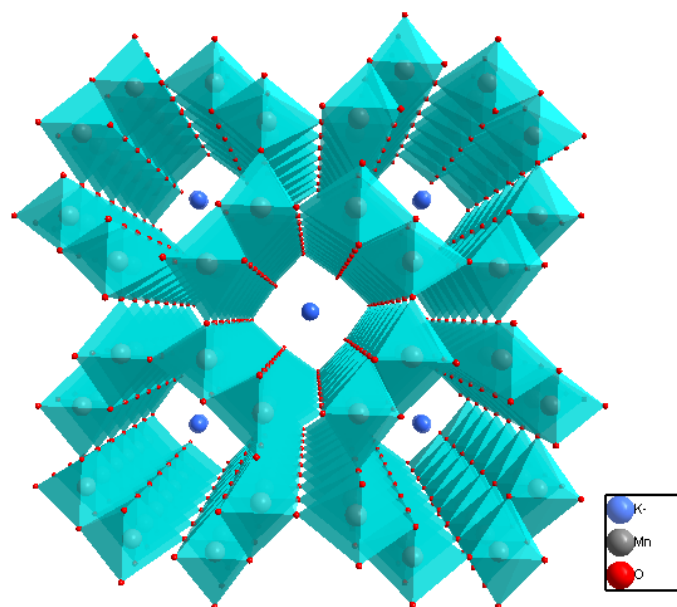


Figure 9. Scheme of the OMS-2 lattice structure

In the above paragraph, we discussed the reason that Sn-OMS-2 have good electrochemical Performance. Now, we explain the difference among the samples. It is generally accepted that the capacitance of MnO_x materials increase with their specific surface area[7]. From the BET results, we know that the surface area of the Sn-OMS-2 materials increased with the Sn dopant rise; therefore, their electrochemical performances show the similar behavior. The 15%Sn-OMS-2 sample show the best performance (187 F/g) with relatively large surface area ($95.4 \text{ m}^2/\text{g}$). For the 20%Sn-OMS-2 sample, its surface area ($108.9 \text{ m}^2/\text{g}$) is larger than that of 15%Sn-OMS-2; however, its capacitance property (146 F/g) is smaller. This is probably caused by the porosity decrease (Fig.7) as too many Sn could fill up with the tunnel of the OMS-2 crystal structure and impede the diffusion of electrolyte cations. The introduced metal into the OMS-2 crystal structure should have an optimum doping amount, too much or too less will not work effectively to enhance the performance. Similar trend has been reported for Fe doped MnO_2 electrode[8].

The 15%Sn-OMS-2 sample is examined at different scan rates as exhibited in Fig.10. Typical CV curves measured at 2, 5 and 10 mV s^{-1} in 1 M Na_2SO_4 electrolyte within voltage range of -0.1 to +0.9 V. The specific capacitance values calculated from the CV profiles decreased from 252 to 218 and 187 F/g with the scan rate rise from 2 to 10 mV s^{-1} . The reason is that the Na^+ or H^+ only reach the outer surface of the electrode at high scan rates, and only the outer active surface is utilized for the charge storage[35].

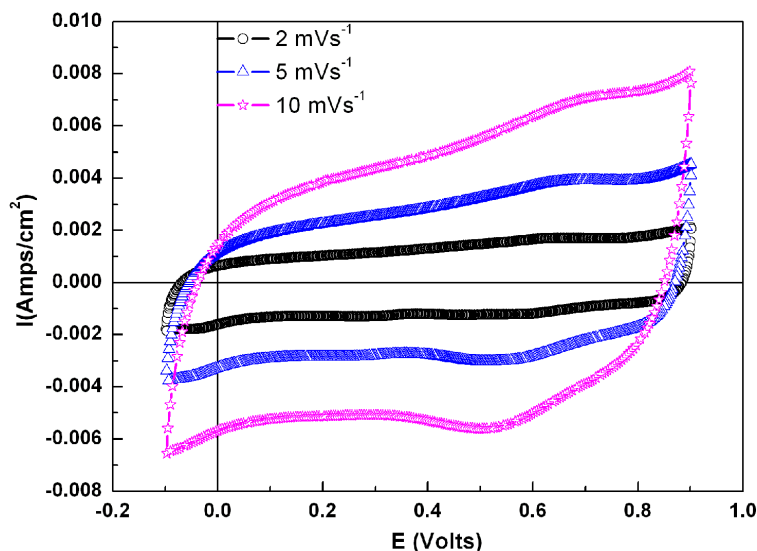


Figure 10. Cyclic voltammograms of 15%Sn-OMS-2 electrode at different scanning rates in 1M Na_2SO_4 (second cycle)

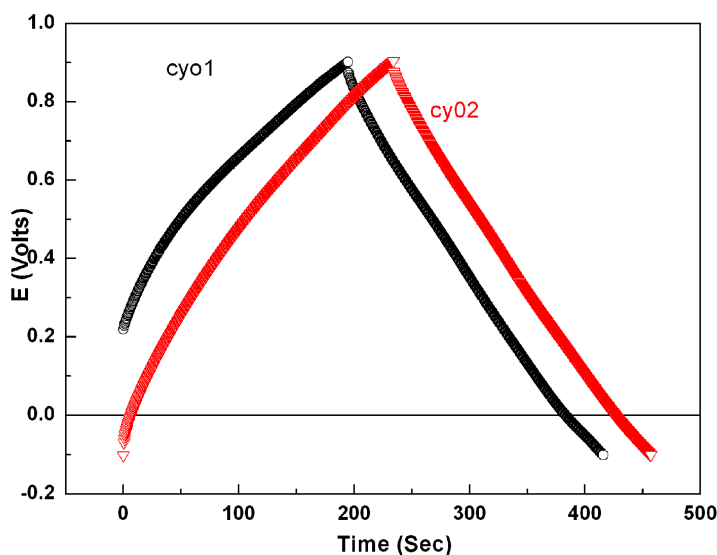


Figure 11. Charge-discharge curves of 15%Sn-OMS-2

The electrochemical activity of 15%Sn-OMS-2 was also investigated by the galvanostatical charge-discharge process (Fig.11). The approximately linear charge-discharge profile indicates that the Sn-OMS-2 materials have regular capacitive behaviors. With charge-discharge curves in Fig. 10, the specific capacitance could be calculated from: $C = I \cdot \Delta t / (m \cdot \Delta V)$, where C , I , t , m and ΔV denote the average specific capacitance, charge-discharge current, charge-discharge time, the mass of powder and the potential difference, respectively. Based on the equation, the average specific capacitance of 15%-Sn-OMS-2 materials is measured to be 185 F/g, which is very much comparable to that gained by the CV curves.

4. CONCLUSION

Sn-doped OMS-2 nanorod materials have been successfully prepared via one-step hydrothermal protocol. The Sn introduction did not change the cryptomelane-like structure of OMS-2 materials. Sn doping was proved by EDX test. The surface area of the OMS-2 materials increased with Sn dopant rise. The lower doping amount (< 10%) of Sn does not have obvious effect on the capacitance performance. Positive effect was found when the doping amount of Sn is larger than 10%, of which 15%Sn-OMS-2 sample exhibited the best supercapacitive property (187 F/g) calculated by the CV curves at a scan rate of 10 mVs⁻¹ in 1 M Na₂SO₄ electrolyte within voltage range of -0.1 to +0.9 V. Such an enhancement was explained from the aspects of crystal structure, conductivity, surface area and pore size.

ACKNOWLEDGEMENT

This work was supported by Natural Science Foundation of Guangdong (10251009001000003), Scientific Program of Guangzhou(2010Z1-E061) and 211 Project of Guangdong Province.

References

1. Y. Zhang, H. Feng, X. Wu, L. Wang, A. Zhang, T. Xia, H. Dong, X. Li, and L. Zhang, *Int. J. Hydrogen Energy*, 34 (2009) 4889.
2. S.H. Li, Q.H. Liu, L. Qi, L.H. Lu, and H.Y. Wang, *Chin. J. Anal. Chem.*, 40 (2012) 339.
3. C. Xu, F. Kang, B. Li, and H. Du, *J. Mater. Res.*, 25 (2011) 1421.
4. W. Wei, X. Cui, W. Chen, and D.G. Ivey, *Chem Soc Rev.*, 40 (2011) 1697.
5. S.L. Suib, *Acc. Chem. Res.*, 41 (2008) 479.
6. P. Ragupathy, D.H. Park, G. Campet, H.N. Vasana, S.J. Hwang, J.H. Choy, and N. Munichandraiah, *J Phys Chem C.*, 113 (2009) 6303.
7. O. Ghodbane, J.L. Pascal, and F. Favier, *ACS Appl Mater Interfaces*, 1 (2009) 1130.
8. D.P. Dubal, and C.D. Lokhande, *Ceram. Int.* (2012)
<http://dx.doi.org/10.1016/j.ceramint.2012.06.042>
9. Y.S. Chen, and C.C. Hu, *Electrochem. Solid-State Lett.*, 6 (2003) A210.
10. G.Y. Zhao, C.L. Xu, and H.L. Li, *J. Power Sources*, 163 (2007) 1132.
11. X. Li, W. Li, X. Chen, and C. Shi, *J. Cryst. Growth*, 297 (2006) 387.
12. M. Nakayama, A. Tanaka, S. Konishi, and K. Ogura, *J. Mater. Res.*, 19 (2011) 1509.
13. M. Nakayama, A. Tanaka, Y. Sato, T. Tonosaki, and K. Ogura, *Langmuir*, 21 (2005) 5907.
14. G. Zhang, L. Zheng, M. Zhang, S. Guo, Z.-H. Liu, Z. Yang, and Z. Wang, *Energy & Fuels*, 26 (2011) 618.
15. J. Wen, X. Ruan, and Z. Zhou, *J. Phys. Chem. Solids*, 70 (2009) 816.
16. Y. Li, and H. Xie, *Ionics*, 16 (2010) 21.
17. X. Pang, Z.Q. Ma, and L. Zuo, *Acta Phys. -Chim. Sin.*, 25 (2009) 2433.
18. H. Kim, and B.N. Popov, *J. Electrochem. Soc.*, 150 (2003) D56.
19. S.N. Pusawale, P.R. Deshmukh, and C.D. Lokhande, *Appl. Surf. Sci.*, 257 (2011) 9498.
20. K. Karthikeyan, S. Amaresh, D. Kalpana, R. Kalai Selvan, and Y.S. Lee, *J. Phys. Chem. Solids*, 73 (2012) 363.
21. C.C. Hu, K.H. Chang, and C.C. Wang, *Electrochim. Acta*, 52 (2007) 4411.
22. I. Shakir, M. Shahid, M. Nadeem, and D.J. Kang, *Electrochim. Acta*, 72 (2012) 134.
23. J. Yan, E. Khoo, A. Sumboja, and P.S. Lee, *ACS Nano*, 4 (2010) 4247.

24. L. Sun, Q. Cao, B. Hu, J. Li, J. Hao, G. Jing, and X. Tang, *Appl. Catal. A*, 393 (2011) 323.
25. [25] E.K. Nyutu, C.H. Chen, S. Sithambaram, V.M.B. Crisostomo, and S.L. Suib, *J Phys Chem C*, 112 (2008) 6786.
26. K. McGuire, Z.W. Pan, Z.L. Wang, D. Milkie, J. Menéndez, and A.M. Rao, *J. Nanosci. Nanotechnol.*, 2 (2002) 499.
27. L. Lamaita, M.A. Peluso, J.E. Sambeth, and H.J. Thomas, *Appl. Catal., B*, 61 (2005) 114.
28. M. Sun, L. Yu, F. Ye, G. Diao, Q. Yu, Y. Zheng, J.Y. Piquemal, *Mater. Lett.* 65 (2011) 3184-3186.
29. X. Tang, J. Li, and J. Hao, *Catal. Commun.*, 11 (2010) 871.
30. K.S.W. Sing, D.H. Everett, R.A.W. Haul, L. Moscou, R.A. Pierotti, J. Rouquerol, and T. Siemieniewska, *Pure Appl. Chem.*, 57 (1985) 603.
31. X. Tang, Y. Li, J. Chen, Y. Xu, and W. Shen, *Microporous Mesoporous Mater.*, 103 (2007) 250.
32. V. Subramanian, H. Zhu, R. Vajtai, P.M. Ajayan, and B. Wei, *J Phys Chem B*, 109 (2005) 20207.
33. V. Subramanian, H. Zhu, and B. Wei, *Chem. Phys. Lett.*, 453 (2008) 242.
34. T. Brousse, M. Toupin, R. Dugas, L. Athouel, O. Crosnier, and D. Belanger, *J. Electrochem. Soc.*, 153 (2006) A2171.
35. Y. Zhang, G.Y. Li, Y. Lv, L.Z. Wang, A.Q. Zhang, Y.H. Song, and B.L. Huang, *Int. J. Hydrogen Energy*, 36 (2011) 11760